JOURNAL OF AIRCRAFT
Vol. 47, No. 6, November–December 2010

Arrival-Time Controllability of Tailored Arrival Subjected to Flight-Path Constraints

Noboru Takeichi* and Daigo Inami†
Nagoya University, Aichi 464, Japan

DOI: 10.2514/1.C000272

Recently, the continuous descent approach has been strongly focused because it can drastically reduce noise emission and fuel consumption during approach. The tailored arrival is proposed to facilitate the continuous descent approach at congested terminal airspace. In a tailored arrival operation, each arriving aircraft is provided with a specifically designed arrival path to fly on a continuous descent approach path without any conflict with other aircraft. In this paper, the arrival-time controllability of the tailored arrival paths determined by the top-of-descent and waypoint positions are discussed. A tailored arrival path is designed using the least number of track-to-fix and radius-to-fix legs neglecting the engine thrust. Two types of tailored arrival path are numerically investigated; one is determined by adjusting the waypoint positions with the fixed top of descent, and the other is determined by top-of-descent position with the fixed waypoints. They are numerically analyzed so as to satisfy a set of appropriate boundary conditions both at the top of descent and landing, and the behavior of the arrival-time difference from the standard continuous descent approach path is explored using a representative set of inputs. The arrival-time controllability is defined as the differences between the fastest and the slowest arrival time. Through several series of arrival-time analyses, it is found that the tailored arrival paths determined by changing the waypoint positions can achieve the larger arrival-time controllability compared with those determined by changing the top-of-descent position. It is also suggested that it is possible to compose an arrival path with the maximum arrival-time controllability without any additional fuel consumption.

Nomenclature

C_{D0}	=	parasite drag coefficient
C_{Di}	=	induced drag coefficient
C_L	=	lift coefficient
g	=	gravity, $g = 9.8$, m/s^2
h	=	altitude, m
m	=	aircraft mass, kg
S	=	aircraft wing area, m^2
v	=	aircraft speed, m/s
x, y	=	aircraft position, m
γ	=	flight-path angle, rad
ρ	=	air density, $\rho = 1.23 \times 10^{-4.56\times10^{-5}h}$, kg/m^3
σ	=	bank angle, rad
ψ	=	azimuth angle, rad

I. Introduction

RECENTLY the continuous descent approach [1] (CDA) has been examined in detail because the aircraft approach noise and the fuel consumption are both drastically reduced [2]. The aircraft approaches the runway with the nearly minimum engine thrust from the cruise altitude in the ideal version of this approach. However it can be difficult to maintain the separation between the aircraft with such small engine thrust in a congested terminal airspace [2] because the uncertainty of the arrival time due to the arrival path deviation of each aircraft is larger than that required for the landing interval in a congested airspace. The tailored arrival (TA) is proposed to facilitate CDA even in such airspace [3]. In TA operation each aircraft is provided with a specifically designed flight-path from the air traffic controller that simultaneously facilitates the separation and the CDA. The TA path is indicated through the fixed waypoints (WPs) and the time to pass them, and the aircraft change the top-of-descent (TOD) position and the flight-path angle to satisfy the indicated arrival time [4]. When a larger or smaller arrival-time control is required, the addition or omission of WPs is also necessary to stretch or reduce the flight-path length [4,5] in addition to the adjustment of the TOD position. It must also be noticed that the TA path with larger flight-path angle for the faster arrival time requires the longer cruise distance, which results in the larger fuel consumption.

Modern aircraft is able to fly on an arbitrary flight-path quite accurately owing to the advanced flight management system and the precise area navigation (RNAV) systems such as the GPS augmentation systems [6]. It is expected that future navigation systems will make it possible to indicate the TA path through arbitrarily determinable WPs unlike the current TA paths. It is also expected that a family of predefined WPs and corresponding TA paths will facilitate a similar TA operation. Concerning the RNAV aided arrival paths, some studies have been carried out for the aircraft noise mitigation [7,8]. In this paper, the arrival-time controllability is especially focused, and it is aimed to clarify the arrival-time difference behavior of the TA paths indicated through the arbitrarily determinable WPs and fixed TOD, compared with the current TA paths indicated through the fixed WPs. Hereafter, the former path is called fixed TOD path, and the latter one is called fixed WP path. The standard CDA path is also defined so that the aircraft descent from the TOD and enter the final glide path through one turning leg. The arrival-time analysis is carried out by comparing the arrival time between the TA paths and the standard CDA path. The arrival paths are designed according to the standard for the RNP approach [9] so that general aircraft are able to fly along it with only small deviations. Through the numerical analyses, it is also aimed to find the TA path definition that provides the optimum arrival-time controllability to facilitate the TA operation even in congested airspace.

II. Flight-Path Composition

As mentioned above, the arrival paths are designed according to the standard [9], and they are composed of radius-to-fix legs (RF legs) and the track-to-fix legs (TF legs). In the standard, an RF leg and

Received 24 January 2010; revision received 1 June 2010; accepted for publication 1 June 2010.

*Associate Professor/Lecturer, Department of Aerospace Engineering, Furocho, Chikusa, Nagoya. Senior Member AIAA.

†Graduate Student, Department of Aerospace Engineering, Furocho, Chikusa, Nagoya.

a TF leg are defined as a constant radius circular path about a defined turn center that terminates at a fix and a geodesic path between two fixes. The standard CDA paths are defined so that the aircraft begins descent from the TOD without changing its cruise flight direction, and enter the final glide path through only one turning leg as shown in Fig. 1a. In this figure, the TF legs and RF leg are denoted as single and double lines, respectively. It is possible to define a family of the standard CDA paths by changing the final glide-path length. The TA paths for the arrival-time control are designed by adding the least number of flight legs to the standard CDA path.

The fixed TOD path is obtained by adding one RF leg and one TF leg and adjusting the final glide-path length. The outline of this path is depicted in Fig. 1b. The standard CDA path and the fixed TOD path are denoted as solid and dashed lines, respectively. Both faster and slower arrival paths are obtained by adjusting the final glide-path (TF3 leg) length. The fixed WP path is designed by adjusting the TOD position as shown in Fig. 1c. This arrangement corresponds to the omission of the RF1 leg of the fixed TOD path, and the arrival-time control is made through the cruise length and the flight-path angles of the TF1 and TF2 legs.

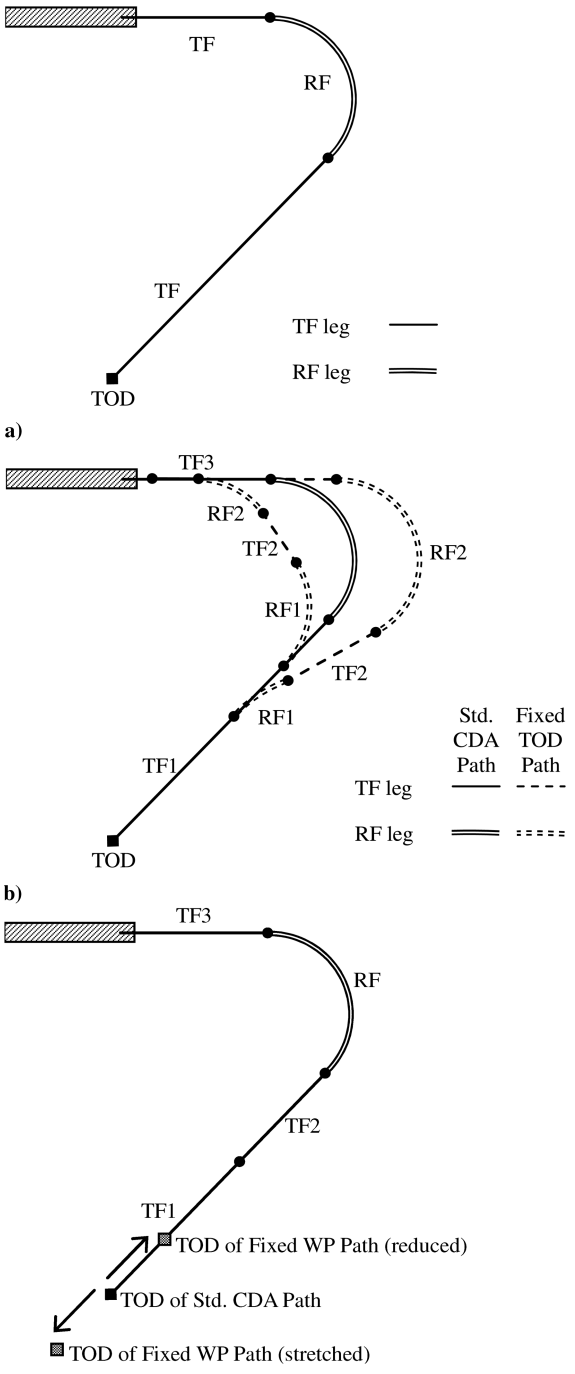

Fig. 1 Outline of arrival paths: a) standard CDA path, b) fixed TOD path, and c) fixed WP path.

Table 1 Aircraft parameters [10]

Parameter	Value
m, kg	2.38×10^5
S, m^2	4.28×10^2
C_{D0}	1.69×10^{-2}
C_{Di}	4.89×10^{-2}
C_{D0} (flap extension)	8.69×10^{-2}
C_{Di} (flap extension)	4.68×10^{-2}

III. Equations of Motion and Boundary Conditions

The TA paths are numerically obtained using the parameters of B777 [10]. The maximum descent gradient and the standard bank angle in RF leg are provided in the standard [9], which are 500 ft per 1 NM and 18 deg, respectively. This descent gradient is equal to -4.7 deg. Therefore the flight-path angle between -4.7 and 0.0 deg and the bank angle of 18 deg in RF leg are applied in the numerical analyses. It is also assumed that the TF3 leg corresponds to the final approach segment, and the flight-path angle is fixed to be -3 deg. The altitude and the velocity are 11,278 m (37,000 ft) and 250 m/s (486 kt) at the TOD, and 305 m (1000 ft) and 80 m/s (156 kt) at the end of TF3 leg. It is also assumed that the flap is extended at the altitude of 610 m (2000 ft).

The TA paths are analyzed so that the aircraft values of state in the equations of motion [Eqs. (1–6)] satisfy the boundary conditions at the TOD and the end of TF3 leg. The TOD position x_{TOD} and y_{TOD} are obtained through the standard CDA path analyses using the boundary conditions Eq. (7) at the TOD and Eq. (9) at the end of TF3 leg. The same boundary conditions [Eqs. (7) and (9)] are used in the fixed WP path analyses. In the fixed TOD path analyses, the same TOD as the standard CDA path given in Eq. (8) is used for the TOD boundary condition. The aircraft parameters are shown in Table 1. For the clarity of the problem, the following two assumptions are made: 1) the engine thrust in idle state is negligibly small and 2) only one flap condition is applied. Although these assumptions do not correspond to the actual ones, they simplify the flight-path analyses, and it is expected that the characteristics of the arrival-time difference will be clearly obtained.

The numerical analyses to solve the boundary value problem and the optimization have been carried by using MATLAB Optimization Toolbox [11]. The dimensionless form of the equations are applied [12], where the time, length, and mass of the state variables are transformed dimensionless by v^*/g, v^{*2}/g, and $\rho^* S v^{*2} C_L^*/2g$, respectively, where the variables with superscript $*$ are the cruise state values. The accuracy of the numerical integration and the boundary condition are $1e-8$ and $1e-6$, respectively:

$$m\frac{\mathrm{d}v}{\mathrm{d}t} = -\frac{1}{2}\rho S(C_{D0} + C_{Di}C_L^2)v^2 - mg\sin\gamma \tag{1}$$

$$mv\frac{\mathrm{d}\gamma}{\mathrm{d}t} = \frac{1}{2}\rho S C_L v^2\cos\sigma - mg\cos\gamma \tag{2}$$

$$mv\frac{\mathrm{d}\psi}{\mathrm{d}t} = \frac{1}{2}\rho S C_L v^2\frac{\sin\sigma}{\cos\gamma} \tag{3}$$

$$\frac{\mathrm{d}h}{\mathrm{d}t} = v\sin\gamma \tag{4}$$

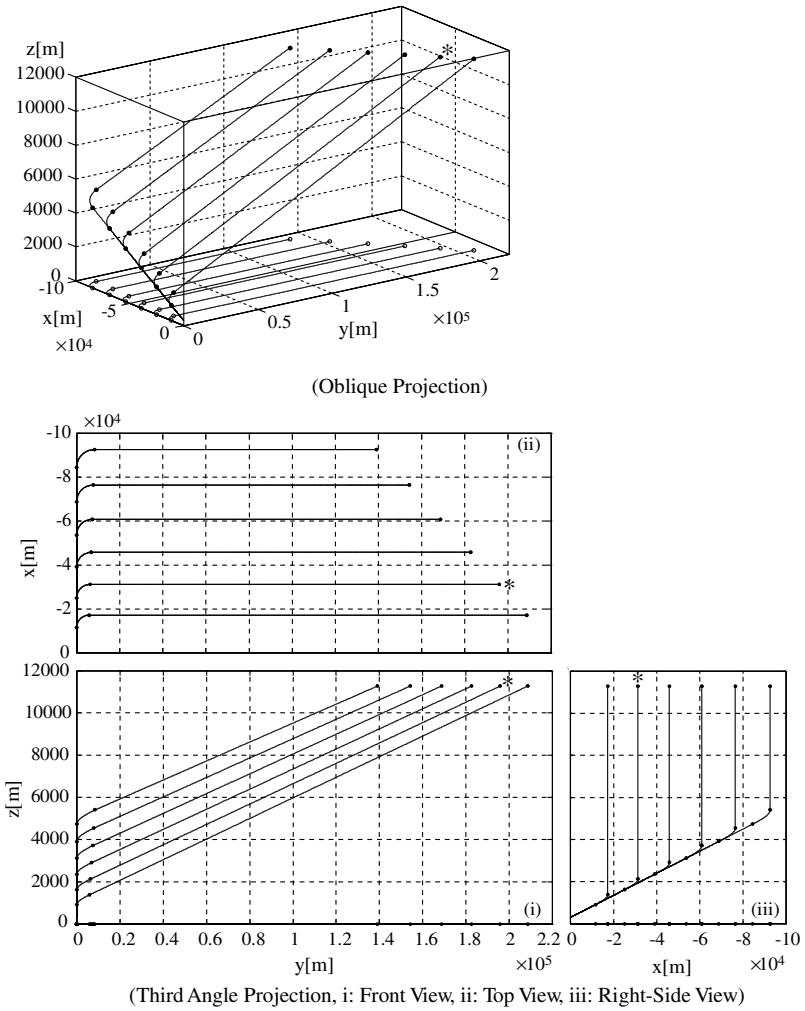

Fig. 2 Standard CDA paths.

$$\frac{dx}{dt} = v\cos\gamma\cos\psi \tag{5}$$

$$\frac{dy}{dt} = v\cos\gamma\sin\psi \tag{6}$$

$$h_{ini} = h^* = 11277.6 \text{ m}(=37000 \text{ ft}), \quad \psi_{ini} = \psi^*, \quad v_{ini} = v^* = 250 \text{ m/s} \tag{7}$$

$$h_{ini} = h^* = 11277.6 \text{ m}(=37000 \text{ ft}), \quad \psi_{ini} = \psi^*, \quad v_{ini} = v^* = 250 \text{ m/s}, \quad x_{ini} = x_{TOD}, \quad y_{ini} = y_{TOD} \tag{8}$$

$$h_{fin} = 304.8 \text{ m}(=1000 \text{ ft}), \quad v_{fin} = 80 \text{ m/s}, \quad \psi_{fin} = 0 \text{ rad}, \quad x_{fin} = 0 \text{ m}, \quad y_{fin} = 0 \text{ m} \tag{9}$$

IV. Arrival-Time Analyses

A. Standard CDA Path

The standard CDA path is analyzed using the −3 deg flight-path angle in both the final glide path and RF leg. It is assumed that the aircraft arrives from the 90 deg azimuth angle from the runway in this paper. A series of the standard CDA paths are obtained by changing the final glide-path length as shown in Fig. 2, where z axis is 10 times magnified. The origin of the x and y axes coincide with the end of the final glide path. The joints of the legs are denoted as circles, and the ground projection of the flight-path is shown as the thin lines.

Table 2 Flight-path angle used in path analyses

Arrival path	TF1	RF1	TF2	RF2	TF3
Faster	γ_1	γ_2	γ_2	−3 deg	−3 deg
Slower	γ_1	γ_2	γ_2	γ_2	−3 deg

B. Arrival-Time Difference Behavior of Fixed TOD Paths

1. Flight-Path Angle

The arrival-time behavior and controllability of the fixed TOD paths is analyzed in this section. The fixed TOD paths are numerically obtained so that they satisfy the same boundary conditions as the standard CDA paths. In this chapter, the standard CDA path with 25 km final glide-path length ($t_{TF3} = 200$ s) is focused as an example, and the arrival-time difference from this standard path is analyzed.

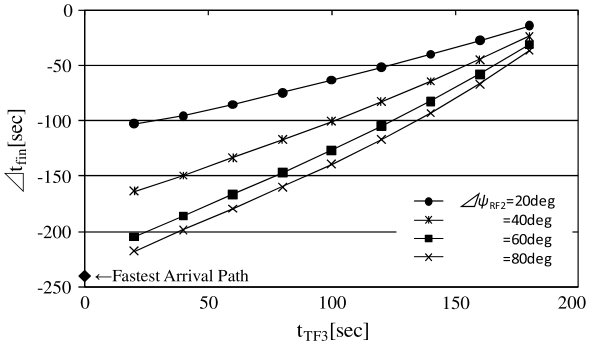

Fig. 3 Faster arrival-time difference.

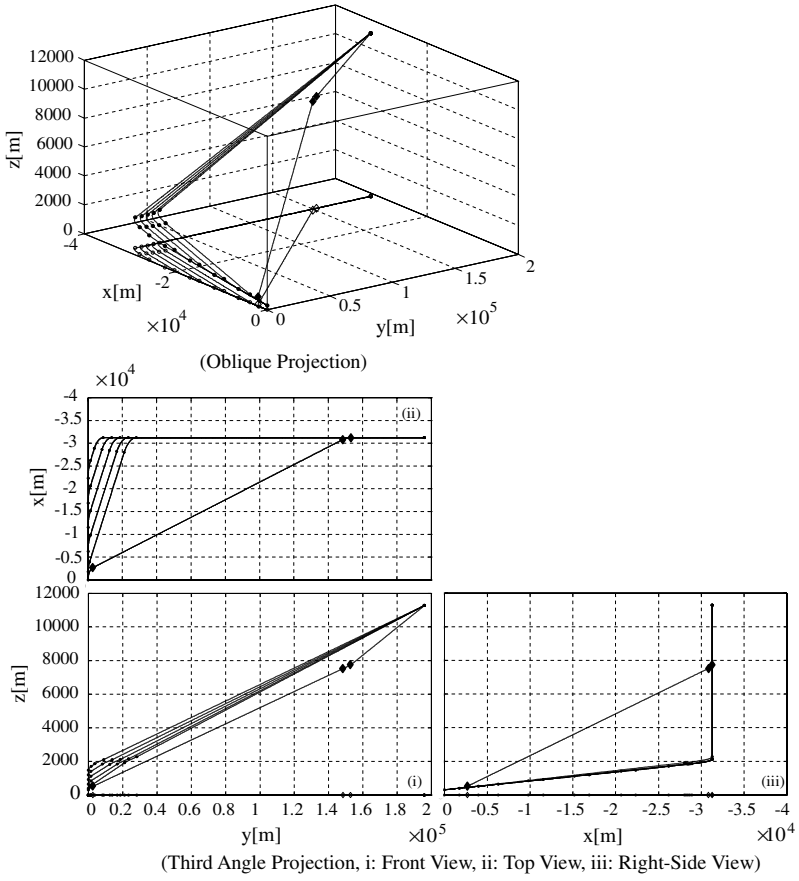

a)

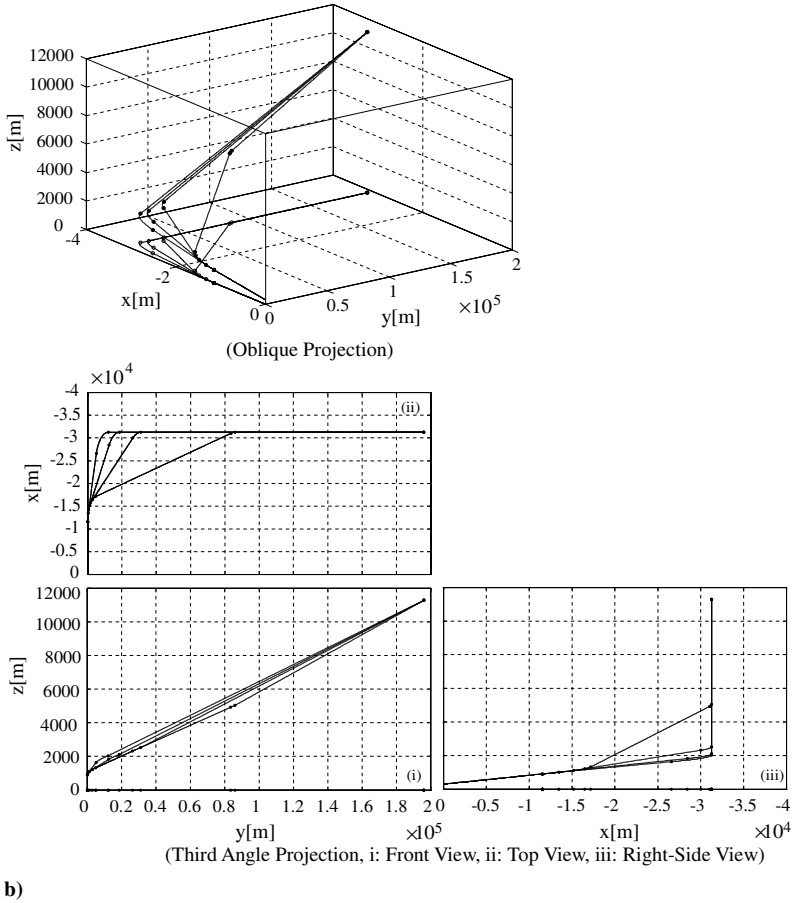

b)

Fig. 4 Faster arrival path: a) $\Delta\psi_{RF2} = 40$ deg, $t_{TF3} = 20 \sim 180$ s (◆: fastest arrival path) and b) $\Delta\psi_{RF2} = 20 \sim 80$ deg, $t_{TF3} = 100$ s.

This path is indicated by $*$ in Fig. 2. The standard CDA flight-path angle of TF1 leg is -2.76 deg, and the standard arrival time is 1241.4 sec. In the arrival-time analyses, the flight-path angles shown in Table 2 are applied. Because the TF3 leg length becomes shorter than that of the standard CDA path in the case of faster arrival path, the -3 deg path angle is applied to the RF2 leg to hold the sufficient flight-path length as the final approach segment.

2. Faster Arrival Path

Faster arrival paths are obtained by shortening the TF3 leg. By determining the RF2 leg turning angle $\Delta\psi_{RF2}$ and the TF3 leg flight time t_{TF3}, a faster arrival path satisfying the boundary conditions is solely obtained. Such a path determination corresponds to the indication of the initial and final points of each leg as the WPs. The difference of the arrival time from the standard path (Δt_{fin}) is analyzed by changing the values of t_{TF3} and $\Delta\psi_{RF2}$. The arrival-time differences are summarized in Fig. 3. It is clearly shown that the larger $\Delta\psi_{RF2}$ and the smaller t_{TF3} enable the faster arrival. The shapes of some typical flight-paths are summarized in Fig. 4, where the x axis and z axis are magnified 5 and 10 times. Figures 4a and 4b show the flight-paths changing the final glide-path length from about 1.75 km to 22.25 km ($t_{TF3} = 20 \sim 180$ s) with the fixed turning angle of $\Delta\psi_{RF2} = 40$ deg, and those changing the RF2 leg turning angle from 20 to 80 deg ($\Delta\psi_{RF2} = 20 \sim 80$ deg) with the fixed final glide-path length 11.5 km ($t_{TF3} = 100$ s), respectively.

When the larger $\Delta\psi_{RF2}$ or the smaller t_{TF3} is given, the horizontal flight distance becomes shorter. The shorter flight distance requires the larger flight-path angle, which results in the faster descent of aircraft as shown in Fig. 3. The flight-path angles γ_1 and γ_2 are separately chosen to satisfy the boundary conditions of the velocity and the altitude. The fastest arrival path is obtained when $t_{TF3} = 0$ s, where the roll out point of the RF2 leg coincides to the point of the final boundary conditions. In this case, $\Delta\psi_{RF2} = 79.1$, $\gamma_1 = -4.70$ and $\gamma_2 = -2.70$ deg, are obtained from the numerical analysis. The fastest path is determined by the final glide-path length limit ($t_{TF3} = 0$ s) and the flight-path angle limit of TF1 ($\gamma_1 = -4.70$ deg), and a possible combination of the $\Delta\psi_{RF2}$ and γ_2 is solely determined to satisfy the boundary conditions. The fastest path is denoted as diamonds (◆) in both Figs. 3 and 4a. Its arrival-time difference from the standard CDA path is $\Delta t_{fin}^{min} = -238.5$ s.

3. Slower Arrival Path

It is also possible to obtain slower arrival paths by extending the TF3 leg. In the same way as the faster arrival paths, a slower arrival path satisfying the boundary conditions is solely determined for a given combination of the larger $\Delta\psi_{RF2}$ or the longer t_{TF3}. The arrival-time difference is summarized in Fig. 5. Some examples of slower arrival paths are shown in Fig. 6. Figures 6a and 6b show the flight-paths changing the final glide-path length from about 26.5 to 29.25 km ($t_{TF3} = 210 \sim 230$ s) with the fixed turning angle of $\Delta\psi_{RF2} = 92.5$ deg, and those changing the RF2 leg turning angle from 92.5 to 100 deg ($\Delta\psi_{RF2} = 92.5 \sim 100$ deg) with the fixed final glide-path length 27.9 km ($t_{TF3} = 220$ s), respectively.

In the case of slower arrival path, when the larger $\Delta\psi_{RF2}$ or the larger t_{TF3} is given, the horizontal flight distance becomes longer. The longer flight distance results in the smaller flight-path angle and slower descent as shown in Fig. 5. The slowest arrival path is obtained when the final glide-path length is 30.1 km ($t_{TF3} = 236.1$ s) and $\Delta\psi_{RF2} = 92.5$ deg, which are denoted as crosses (+) in Figs. 5 and 6a. In this case, the flight-path angles are $\gamma_1 = -2.07$ and $\gamma_2 = -3.03$ deg, and the arrival-time difference from the standard path is $\Delta t_{fin}^{max} = 127.9$ s. In the slowest arrival path, the aircraft dissipates its kinetic energy by flying on the path with as small flight-path angle as possible with satisfying the boundary conditions. Therefore, if the aircraft flies on even a slightly longer flight-path than the slowest path or a TF1 leg with a slightly smaller flight-path angle than that for the slowest path $\gamma_1 = -2.07$ deg, the aircraft cannot maintain the velocity to satisfy the final boundary conditions. It is considered the slowest arrival path depicted in Fig. 6a has the longest flight distance that satisfies the boundary conditions.

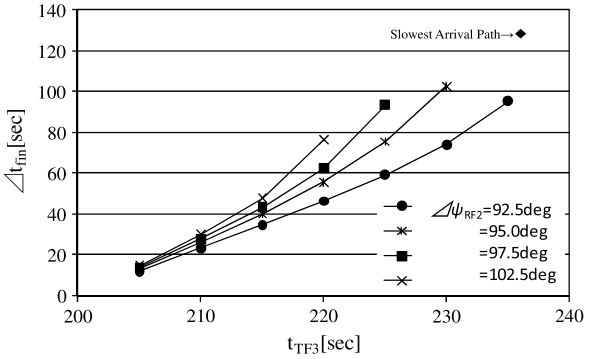

Fig. 5 Slower arrival-time difference.

C. Arrival-Time Difference Behavior of Fixed WP Paths

The fixed WP paths are obtained by moving the TOD in the arrival direction as shown in Fig. 1c. Slower arrival path is obtained by shortening the cruise length and applying the smaller flight-path angle. The faster arrival path is obtained by extending the cruise length and applying the larger flight-path angle. The fixed WP paths are analyzed by finding a combination of γ_1 and γ_2 to satisfy the boundary conditions.

The fastest, slowest and standard paths are shown in Fig. 7 denoted as ◆, + and •, respectively. In the fastest arrival path, $\gamma_1 = -4.70$ and $\gamma_2 = -0.00$ deg, which means that the fastest path is determined by the limitation of the flight-path angle. In this case, the aircraft flies on TF1 leg with the large flight-path angle limit ($\gamma_1 = -4.70$ deg) for the fastest descent, and flies on TF2 leg with the small flight-path angle limit ($\gamma_2 = -0.00$ deg) for the most rapid deceleration to satisfy the final boundary conditions. The flight-path angles in the slowest path are $\gamma_1 = -2.52$ and $\gamma_2 = -3.54$ deg. As mentioned in the slowest fixed TOD path case, the aircraft dissipates its kinetic energy by flying on the path with as small flight-path angle as possible with satisfying the boundary conditions. Therefore, it is impossible to satisfy the final boundary velocity condition by flying on the TF1 leg with even a smaller flight-path angle than that for the slowest path. The cruise lengths of the fastest and slowest paths are 50.4 km longer and 3.63 km shorter than that of the standard CDA path, respectively. The cruise time difference should also be considered in the arrival-time analyses using the following equation:

$$\Delta t_{fin} = \Delta t_{fin}^{TOD} - \frac{\Delta TOD\ [m]}{v_{ini}\ [m/s]} = \Delta t_{fin}^{TOD} - \frac{\Delta TOD\ [m]}{250\ [m/s]} \tag{10}$$

where Δt_{fin}^{TOD} is the arrival time measured from the TOD. The arrival-time differences obtained from the Eq. (9) were $\Delta t_{fin}^{min} = -204.5$ s for the fastest arrival path, and $\Delta t_{fin}^{max} = 94.3$ s for the slowest arrival path. In addition, it must be noticed that the amount of the fuel is also changed due to the cruise length change. Especially this result in the additional fuel consumption in faster arrival paths. The fuel consumption rate of the B777 aircraft is 117.5 kg/min for the cruise at the altitude 37,000 ft [10], which is equal to 7.83 kg/km. In this case, the fastest path requires 395 kg fuel in addition to the standard CDA path or the fixed TOD path. On the other hand, the slowest path can achieve almost the same arrival-time delay as the fixed TOD path with diminishing the fuel consumption about 28 kg.

V. Arrival-Time Controllability

It is possible to define the arrival-time controllability as the difference between the fastest arrival time Δt_{fin}^{min} and the slowest one Δt_{fin}^{max}. The maximum arrival-time differences Δt_{fin}^{min} and Δt_{fin}^{max}, and the controllability $\Delta t_{fin}^{max} - \Delta t_{fin}^{min}$ are summarized in Fig. 8. In this case, the arrival-time difference and the controllability of the standard CDA paths with the final glide-path length of $0 \sim 84.4$ km ($t_{TF3} = 0 \sim 600$ s) are analyzed. The vertical axes denote the arrival-time difference from the standard CDA paths in Fig. 8a, and the arrival-time controllability in Fig. 8b.

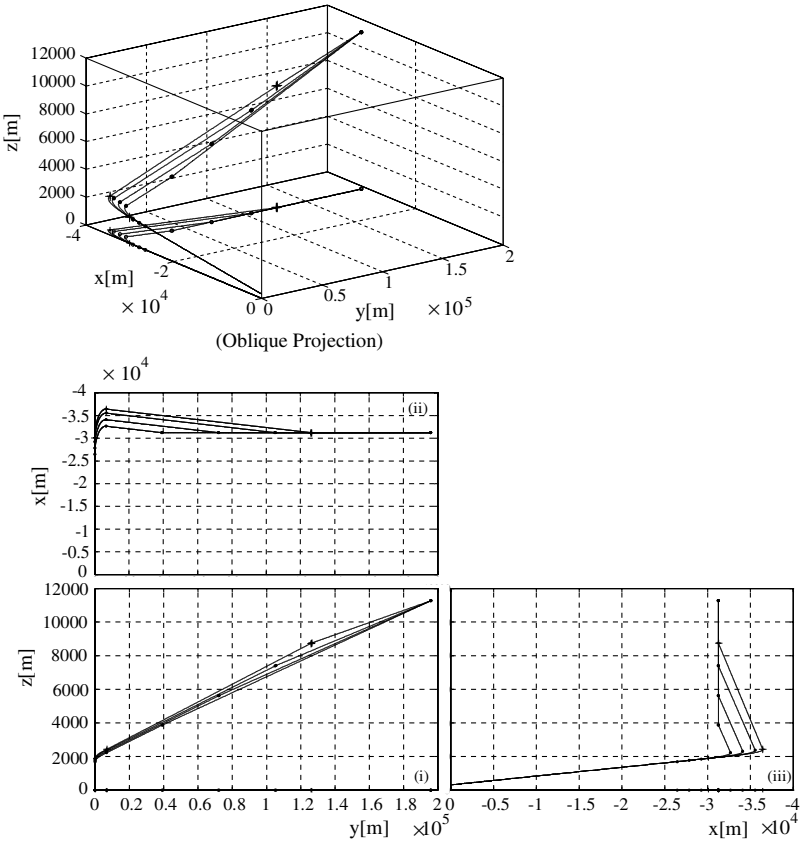

a)

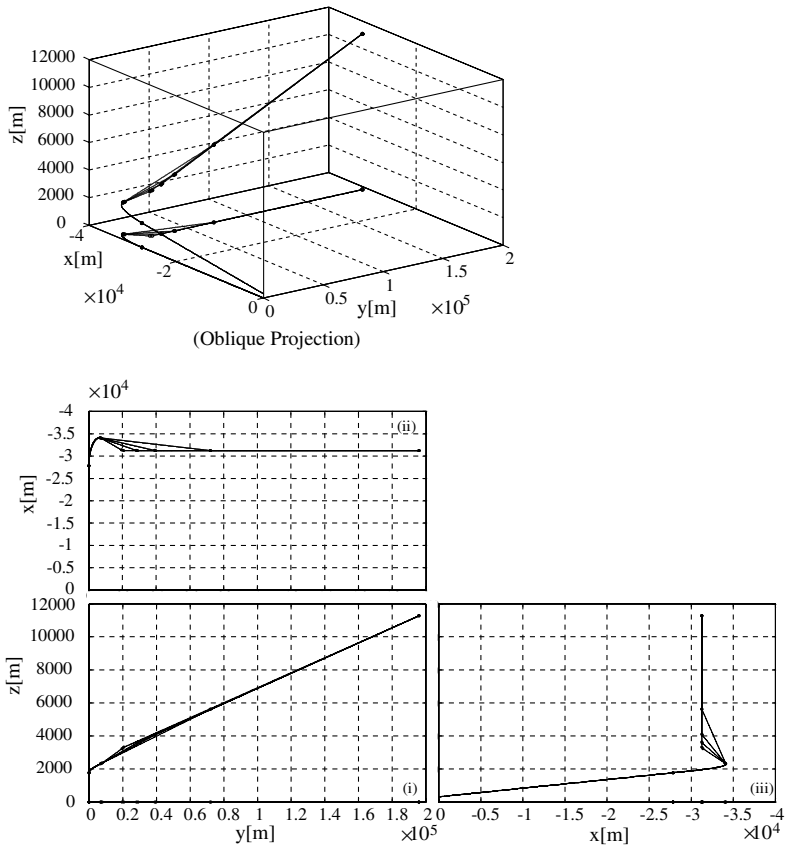

b)

Fig. 6 Slower arrival path: a) $\Delta\psi_{RF2} = 92.5$ deg, $t_{TF3} = 210 \sim 230$ s (+: slowest arrival path) and b) $\Delta\psi_{RF2} = 92.5 \sim 100$ deg, $t_{TF3} = 220$ s.

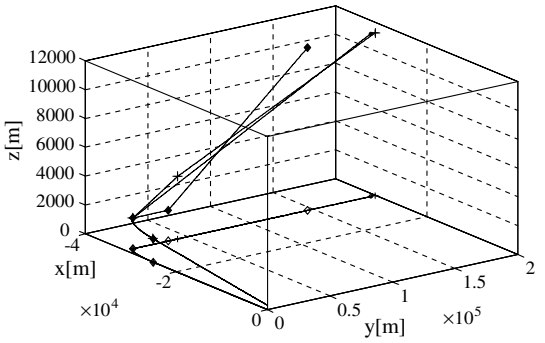

(Oblique Projection)

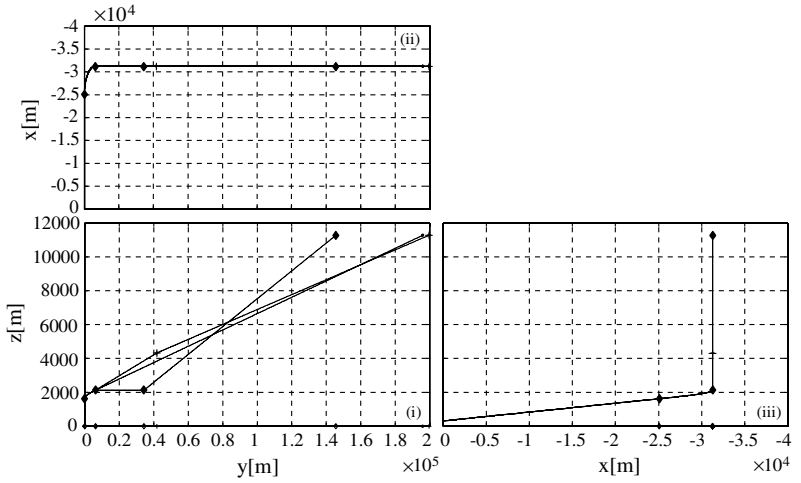

(Third Angle Projection, i: Front View, ii: Top View, iii: Right-Side View)

Fig. 7 Fixed WP path (◆: fastest arrival path; +: slowest arrival path; ●: standard CDA path).

In Fig. 8a, the lines A and B denote the slowest and fastest arrival-time differences of the fixed TOD paths, and the lines C and D denote those of the fixed WP paths, respectively. The lines E and F in Fig. 8b denote the arrival-time controllability of the fixed TOD path and the fixed WP path.

It is found that the arrival-time difference of the fastest fixed TOD path (denoted by line B) becomes larger as the longer final glide path is applied. On the contrary, the arrival-time difference of the fastest fixed WP path (denoted by line D) becomes smaller. Both of the Fixed TOD and Fixed WP fastest arrival paths are obtained when the flight-path angles coincide with the limit values. In the Fixed WP path, the aircraft rapidly descents on the path of $\gamma_1 = -4.70$ deg, and flies on the path of $\gamma_2 = 0.00$ deg to satisfy the boundary conditions as shown in Fig. 7. In the Fixed TOD path, the aircraft rapidly descents on the path of $\gamma_1 = -4.70$ deg similarly, and flies on the smaller flight-path angle to satisfy all of the boundary conditions simultaneously as shown in Fig. 4a. The TF1 leg length decreases as the final glide-path length increases. The faster arrival-time difference of the fixed WP path also decreases because the arrival-time control is made mainly by the flight-path angle of the TF1 leg. On the other hand, the faster arrival-time difference of the fixed TOD path increases because the path length difference between the standard and the fastest path length becomes larger. However the path length difference turns to decrease as the final glide-path length further increases, and the increase rate of the faster arrival-time difference becomes smaller as shown in Fig. 8 line B.

Both of the arrival-time difference of the slowest Fixed TOD (line A) and Fixed WP (line C) paths are almost the same values and decrease in almost the same manner. As mentioned above, the slowest arrival path is determined so that the aircraft dissipates its mechanical energy as long as possible with satisfying the boundary conditions. Hence there are small differences between the slowest arrival times of the Fixed TOD and fixed WP paths. Because the arrival time of the standard CDA path with longer final glide path becomes larger while the slowest arrival time hardly differ, the

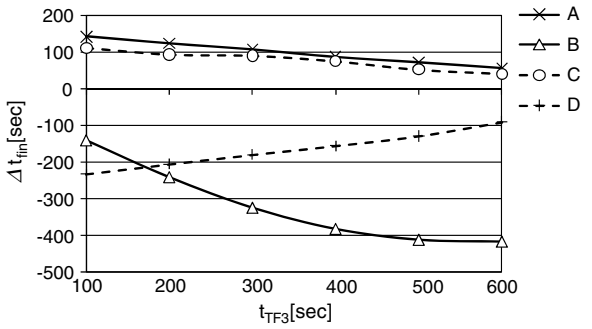

A: Slowest Fixed TOD Path, B: Slowest Fixed TOD Path,
C: Slowest Fixed WP Path, D: Slowest Fixed WP Path

a)

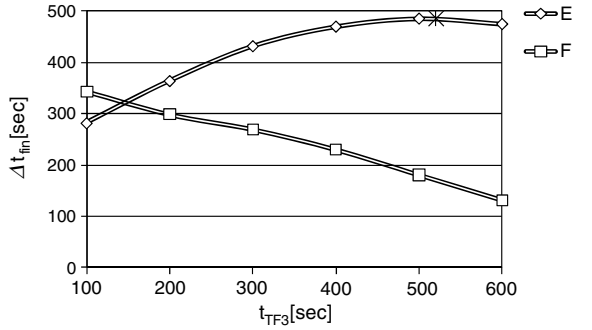

E: Arrival Time Controllability of Fixed TOD Path,
F: Arrival Time Controllability of Fixed WP Path

b)

Fig. 8 Arrival-time difference and controllability: a) fastest and slowest arrival-time differences and b) arrival-time controllability (∗: maximum controllability).

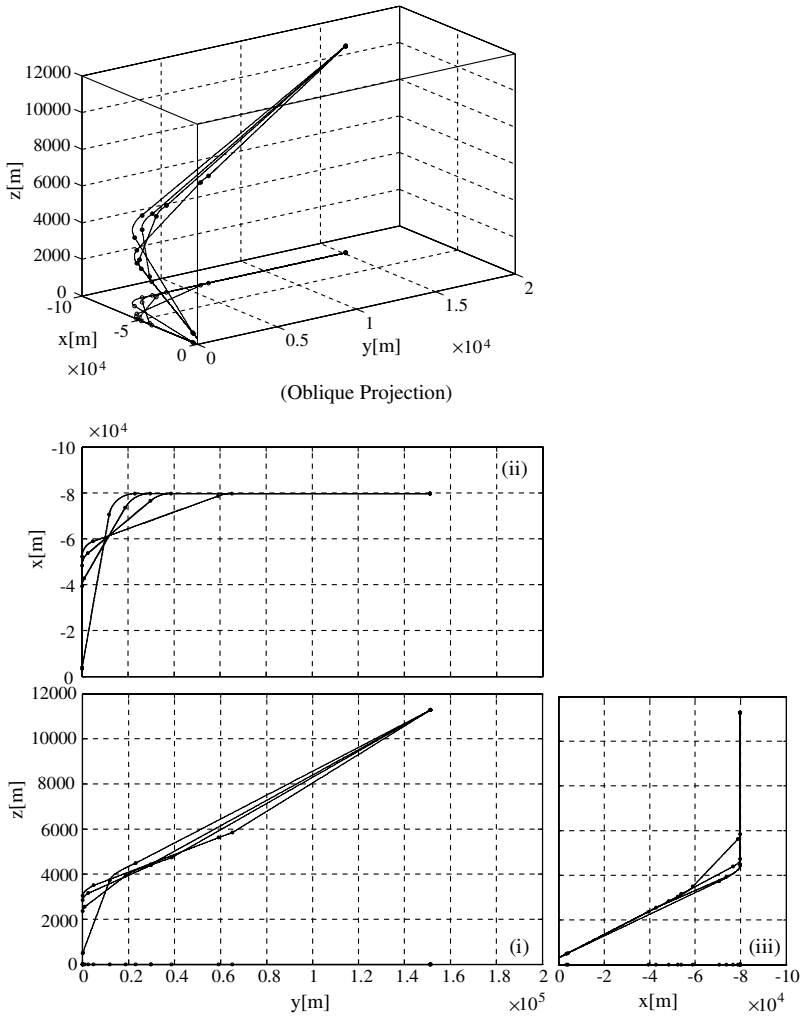

Fig. 9 Arrival paths with maximum arrival-time controllability.

difference between the slowest arrival time and the standard one monotonously decreases as shown in Fig. 8 Line A and C.

Because the faster arrival-time difference increases with its rate decreasing, and the slower arrival-time difference monotonously decreases in the case of the fixed TOD paths, the arrival-time controllability has a maximum value as shown in line E. Through the quadratic interpolation, it is clarified the maximum controllability is realized when $t_{TF3} = 520.5$ s, which is indicated by $*$ in Fig. 8. By defining the flight-path with the arrival-time difference of $\Delta t_{fin} = -172.5$ s as the standard arrival path, the maximum controllability of ± 242.6 s is achieved.

It is possible to compose a series of the arrival path with the maximum controllability by determining the combinations of the path parameters t_{TF3} and $\Delta\psi_{RF2}$. Figure 9 shows several arrival paths with the RF2 leg turning angle from 20 to 80 deg ($\Delta\psi_{RF2} = 20 \sim 80$ deg), where the z axis is 10 times magnified. In this way, it is possible to compose various arrival path with the same maximum controllability. Therefore, it is expected to be possible to achieve the maximum controllability and the noise abatement simultaneously by composing the arrival path avoiding residential area. It will also be possible to achieve the maximum controllability and the obstacle clearance by composing the arrival path avoiding large obstacles, such as tall buildings, mountains, etc.

VI. Conclusions

The arrival-time behavior and its controllability of two types of the TA paths have been discussed in this paper. The arrival paths are composed of TF and RF legs so that the general aircraft can easily follow them. It has been clarified that the fixed TOD paths can achieve the larger time controllability than the fixed WP paths. In addition, it is possible to control the arrival time of the fixed TOD path without any additional fuel consumption, in contrast to the conventional fixed WP path which inevitably requires the additional fuel consumption for faster arrival-time control.

The arrival path with the maximum controllability is also proposed. It is possible to maximize the arrival-time controllability of the TA operation by having aircraft arrive toward the TOD of the arrival path with the maximum controllability, and indicating a TA path to satisfy the required time of arrival. In addition, the arrival path with the maximum controllability still has 1 degree of freedom in path structure as shown in Fig. 9. Therefore it is further possible to compose the standard arrival route considering other conditions, such as the noise abatement, the obstacle clearance, etc. Through the arrival-time analyses, it has also been shown that it is possible to compose the faster arrival path by the fixed TOD path without any additional fuel consumption, and that it is possible to compose the slower arrival path by the fixed WP path with reducing the fuel consumption. Therefore the simultaneous optimization of the arrival-time controllability and the fuel reduction is also possible by the combination of the faster fixed TOD path and the slower fixed WP path.

This paper has discussed the arrival-time controllability determined by the flight-path composition with the least number of flight legs through numerical analyses using only one type of aircraft parameter. Therefore, to show the feasibility and practical usefulness

of the presented concept, more detailed analyses considering various aircraft types, actual flight procedures such as flap setting and near idle thrust state, speed limitations, boundary conditions at TOD and landing, etc., are indispensable in future works. In addition, it is also expected that the further larger arrival-time controllability will be achieved by using a larger number of flight legs. It is also necessary to confirm the advantage of the arrival path with the maximum arrival-time controllability in the cases where the aircraft arrives from all the azimuth angle. The effects of many causes of the flight-path deviation, such as the aircraft parameters, the navigational and the flight technical errors, the atmospheric conditions, etc, must also be investigated to show the feasibility of the presented TA procedure.

References

[1] Clarke, J-P. B., Ho, N. T., Ren, L., Brown, J. A., Elmer, K. R., Tong, K.-O., and Wat, J. K., "Continuous Descent Approach: Design and Flight Test for Louisville International Airport," *Journal of Aircraft*, Vol. 41, No. 5, 2004, pp. 1054–1066. doi:10.2514/1.5572

[2] Erkelens, L. J. J., "Research on Noise Abatement Procedures," National Aerospace Lab., Rept. NLR-TP-98066, Feb. 1998.

[3] Coppenbarger, R. A., Mead, R. W., and Sweet, D. N., "Field Evaluation of the Tailored Arrivals Concept for Datalink-Enabled Continuous Descent Approach," Seventh AIAA Aviation Technology, Integration, and Operations Conference, AIAA Paper 2007-7778, Belfast, Northern Ireland, 18–20 Sept. 2007.

[4] Coppenbarger. R., Lanier, R., Sweet, D., and Dorsky, S., "Design and Development of the En-Route Descent Advisor for Conflict Free Arrival Metering," AIAA Guidance, Navigation, and Control Conference, AIAA Paper 2004-4875, Providence, RI, Aug. 2004.

[5] Ren, L., and Clarke, J. P. B., "Flight-Test Evaluation of the Tool for Analysis of Separation and Throughput," *Journal of Aircraft*, Vol. 45, No. 1, Jan.–Feb. 2008, pp. 323–332. doi:10.2514/1.30198

[6] Grewal, M. S., Weill, L. R., and Andrews, A. P., *Global Positioning Systems, Inertial Navigation, and Integration*, Wiley, Hoboken, NJ, 2007, pp. 199–254.

[7] Prats, X., Nejjari, F., Puig, V., Quevedo, J., and Mora-Camino, F., "A Framework for RNAV Trajectory Generation Minimizing Noise Nuisances," Second International Congress on Research in Air Transportation, Belgrade, Serbia, 2006.

[8] Prats, X., Quevedo, J., and Puig, V., "Trajectory Management for Aircraft Noise Mitigation Towards Future ATM/CNS," ENRI International Workshop on ATM/CNS, Tokyo, Japan, 5–6 March 2009.

[9] FAA, "United States Standard for Required Navigation Performance Approach Procedures with Special Aircraft and Aircrew Authorization Required (RNP-SAAAR)," Order 8260.52, 5 June 2005, http://www.airweb.faa.gov [retrieved 10 June 2009].

[10] Eurocontrol Experimental Center, "User Manual for the Base of Aircraft Data (BADA) Revision 3.7," EEC TR 2009-003, March 2009, (http://www.eurocontrol.int/eec/public/standard_page/proj_BADA.html).

[11] The MathWorks, "Optimization Toolbox 5 User's Guide," http://www.mathworks.com/ [retrieved 15 June 2009].

[12] Tsuchiya, T., "Near-Optimal Guidance Method for Maximizing the Reachable Domain of Gliding Aircraft," *Transactions of the Japan Society for Aeronautical and Space Sciences*, Vol. 49, No. 165, 2006, pp. 137–145. doi:10.2322/tjsass.49.137